Applied Clay Science 101 (2014) 604–607

Contents lists available at ScienceDirect

Applied Clay Science

journal homepage: www.elsevier.com/locate/clay

Research paper

Using Agrawal integral equation to study the pyrolysis kinetics of exfoliated montmorillonite from a polyhedral oligomeric silsesquioxane surfactant and click chemistry

Hui-Wang Cui [a,b,*], Shiao-Wei Kuo [a]

[a] Department of Materials and Optoelectronic Science, National Sun Yat-Sen University, Kaohsiung 804, Taiwan
[b] Institute of Scientific and Industrial Research, Osaka University, Ibaraki 565-0047, Osaka, Japan

ARTICLE INFO

Article history:
Received 29 April 2014
Received in revised form 12 September 2014
Accepted 18 September 2014
Available online 6 October 2014

Keywords:
Nanocomposites
Polyhedral oligomeric silsesquioxane
Pyrolysis kinetics

ABSTRACT

In this study, the exfoliated montmorillonite was prepared through the click chemistry of a propargyl-containing intercalator with singly or multiply azido-functionalized polyhedral oligomeric silsesquioxane nanoparticles. Thermogravimetric analyses revealed that the pyrolysis kinetics had a close relationship to the layered structures, exfoliated structures, and cage-like molecules of polyhedral oligomeric silsesquioxane nanoparticles. The pyrolysis of exfoliated montmorillonite had a mechanism function of Avrami–Erofeev equation, and the kinetic compensation effect equation revealed the pyrolysis.

1. Introduction

As a cheap, natural nanomineral, montmorillonite (Mt) has been used widely in many polymers, such as epoxy (Ha et al., 2008; Lakshmi et al., 2008; Nuhiji et al., 2011), polyethylene (Liang et al., 2004; Xu et al., 2004; Qian et al., 2007), polypropylene (Liu et al., 2010; Martin et al., 2010; Dolomanova et al., 2012), polyurethane (Yu et al., 2008; Qiao et al., 2009; Wang et al., 2009), polybenzoxazine (Takeichi et al., 2002; Fu et al., 2008; Demir et al., 2011; Vengatesan et al., 2011), ethylene-vinyl acetate (Bee et al., 2012; Chen et al., 2012; Hwang et al., 2012), and polyvinyl acetate (Cui and Du, 2011a,b,c, 2012a,b,c, 2013a), to improve the chemical, physical, mechanical, and thermal properties because of its special layered structure and excellent dispersion, water-swelling, thixotropy, adhesion, ion exchange capacity, and organic adsorption behavior. Therefore, many technologies have been developed accordingly to prepare such polymer nanocomposites (Teixeira et al., 2011; Touchaleaume et al., 2011; Zhang et al., 2011; Greesh et al., 2012; Zhu et al., 2012). In our previous work, we used click chemistry to react singly and multiply functionalized azido-polyhedral oligomeric silsesquioxanes (N_3-POSS) with a propargyl-containing, long-alkyl-chain intercalator to prepare organic/inorganic hybrid surfactants for the exfoliation of Mt (Cui and Kuo, 2012, 2013a,b, 2014). The cage-like molecules of polyhedral oligomeric silsesquioxanes (POSS) presenting organic substituents on the outer surfaces (Fig. 1) had exfoliated the Mt into single layers. Their structures and thermal properties were investigated except the pyrolysis kinetics.

Agrawal integral equation can be used to analyze the pyrolysis kinetics of polymers and their composites (Agrawal, 1987; Hu and Shi, 2001). In our previous work, the glass transition kinetics (Cui and Du, 2012d, 2013b), cold crystallization kinetics (Cui and Du, 2012d, 2013b), and pyrolysis kinetics (Cui and Du, 2013c; Fang et al., 2013) of the exfoliated nanocomposites from vinyl acetate and organic Mt were studied using Agrawal integral equation. In this study, we reacted *N*,*N*-dimethylstearylamine with propargyl bromide and then used the product to prepare intercalated Mt (In-Mt); subsequently, we incorporated a POSS derivative functionalized with azido groups into the opened layers of In-Mt, where it reacted with the intercalator through click chemistry to form exfoliated Mt (Ex-Mt). The pyrolysis kinetics of Ex-Mt was investigated using Agrawal integral equation, and the related influence from the cage-like molecules of POSS nanoparticles was discussed also.

2. Experiments

2.1. Samples

The pristine Mt was purchased from Nanocor (USA). The In-Mt and Ex-Mt were obtained according to previously reported procedures (Cui and Kuo, 2012, 2013a,b, 2014). The In-Mt was prepared from pristine Mt, *N*,*N*-dimethylstearylamine, and propargyl bromide. The Ex-Mt-A was prepared from In-Mt and mono-functionalized azide-POSS, and the Ex-Mt-B from In-Mt and multi-functionalized azide-POSS.

* Corresponding author at: Institute of Scientific and Industrial Research, Osaka University, Ibaraki 565-0047, Osaka, Japan. Tel.: +81 6 6879 8521; fax: +81 6 6879 8522.
E-mail address: cuihuiwang@hotmail.com (H.-W. Cui).

http://dx.doi.org/10.1016/j.clay.2014.09.026

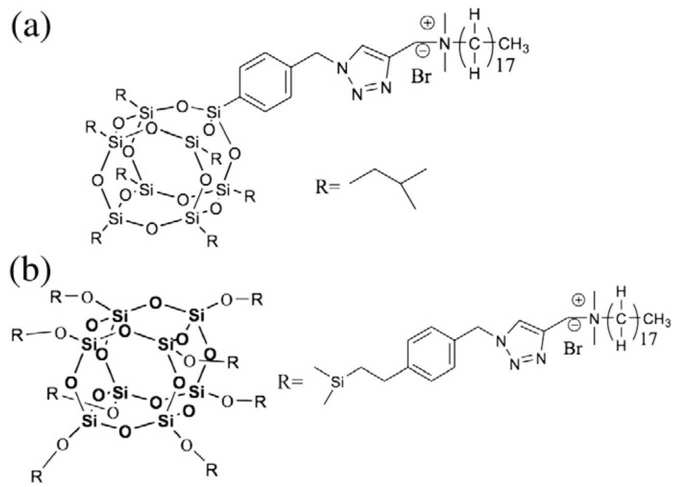

Fig. 1. (a) Mono-functionalized POSS presenting an organic substituent and (b) multi-functionalized POSS presenting eight organic substituents on the outer surfaces after click reactions.

2.2. Characterization

Wide-angle X-ray diffraction (WAXD) data were collected using a BL17A1 wiggler beam line of the National Synchrotron Radiation Research Center (NSRRC), Taiwan. A triangular bent Si (111) single crystal was employed to obtain a monochromated beam having a wavelength (λ) of 1.33001 Å. The value of $d_{(001)}$ was calculated using Bragg's law. The thermal stabilities of the samples were measured using a TA Q-50 thermogravimetric analyzer (TGA) operated under a pure N_2 atmosphere. The sample (ca. 7 mg) was placed in a Pt cell and heated at a rate of 20 °C·min^{-1} from 30 to 800 °C under a N_2 flow rate of 60 ml·min^{-1}. Transmission electron microscopy (TEM) images were recorded using a JEOL-2100 transmission electron microscope operated at an accelerating voltage of 200 kV. Ultrathin sections (thickness: ca. 70 nm) of the TEM samples were prepared using a Leica Ultracut UCT microtome equipped with a diamond knife; they were then placed onto Cu grids coated with carbon-supporting films.

3. Results and discussion

About the pyrolysis kinetics, the mechanism function is expressed as:

$$G(a) = \frac{A}{\beta}\int_{T_0}^{T} e^{-\frac{E}{RT}}\mathrm{d}T.$$

The Agrawal approximate equation is (Agrawal, 1987):

$$\int_{T_0}^{T} e^{-\frac{E}{RT}}\mathrm{d}T = \frac{RT^2}{E}\left[\frac{1-\left(\frac{RT}{E}\right)}{1-5\left(\frac{RT}{E}\right)^2}\right]e^{-\frac{E}{RT}}.$$

Combining the above two equations together, the Agrawal integral equation is written as:

$$ln\left[\frac{G(a)}{T^2}\right] = ln\left\{\frac{AR}{\beta E}\left[\frac{1-\left(\frac{RT}{E}\right)}{1-5\left(\frac{RT}{E}\right)^2}\right]\right\} - \frac{E}{RT}.$$

For the general reaction temperatures and most of E, the relationship among E, R, and T is:

$$\frac{E}{RT} >> 1, 1-\left(\frac{RT}{E}\right) \approx 1, \text{ and } 1-5\left(\frac{RT}{E}\right)^2 \approx 1.$$

The Agrawal integral equation is simplified as:

$$ln\left[\frac{G(a)}{T^2}\right] = ln\left(\frac{AR}{\beta E}\right) - \frac{E}{RT}.$$

The relationship between $ln\left[\frac{G(a)}{T^2}\right]$ and $\frac{1}{T}$ will be linear with a suitable $G(a)$, then E can be calculated from the linear slope and A from the linear intercept. In the above equations, T (K) is the temperature, R is the universal gas constant of 8.314 J·(mol·K)$^{-1}$, β is the heating rate of 20 °C·min^{-1}, E (kJ·mol^{-1}) is the active energy, A (min^{-1}) is the frequency factor, and a is the relative weight loss calculated by:

$$a = \frac{m_i - m_T}{m_i - m_f}$$

where m_i is the initial weight, m_f is the final weight, and m_T is the weight at T.

According to the simplified Agrawal integral equation, T and a in the pyrolysis phases [Fig. 2(a)] were linear fit using a trial-and-error method (Hu and Shi, 2001), as shown in Tables S1, S2, S3, and S4. On the basis of the correlation coefficient, the pyrolysis kinetics of pristine Mt, In-Mt, Ex-Mt-A, and Ex-Mt-B was obtained, as shown in Table 1. In these kinetic parameters, $G(a)$ is the kinetics mechanism function to illustrate the pyrolysis process. If the $G(a)$ is different, the linear fit equation, correlation coefficient, E, A, and reaction order are definitely different also. As Table 1 shows, the $G(a)$ for pristine Mt and In-Mt was Zhuralev–Lesokin–Tempelman equation with a mechanism of three-dimensional diffusion, 3D; and the $G(a)$ of Avrami–Erofeev equation and the mechanism of random nucleation and subsequent growth for Ex-Mt-A and Ex-Mt-B. The differences on $G(a)$ were caused by their respective different structures, e.g. Mt and In-Mt with layered structure, and Ex-Mt-A and Ex-Mt-B with exfoliated structure. The WAXRD pattern of pristine Mt featured a peak at 5.38°, corresponding to a basal space of 1.42 nm; that of In-Mt exhibited a diffraction angle at 2.05°, corresponding to a basal space of 3.73 nm (Fig. S1) (Cui and Kuo, 2012, 2013a,b, 2014). This implies that the pristine Mt and In-Mt both had the layered structure, confirmed by the TEM images [Fig. S2(a) and (b)]. While no diffraction peaks appeared within the range of 0.5–5° in the WAXRD patterns of Ex-Mt-A and Ex-Mt-B, indicating that the Mt had been exfoliated completely as a result of the click reactions (Figs. S1 and S2). The diffraction peaks at approximately 5° embodied the crystal characteristics of the POSS moieties, confirming that the mono- and multi-functionalized azide-POSS derivatives had indeed entered between the layers of In-Mt and underwent subsequent click reactions with the acetylene groups of intercalation agents, resulting in strong exfoliation of Mt (Fig. S1) (Cui and Kuo, 2012, 2013a,b, 2014). The TEM images of Ex-Mt-A [Fig. S2(c)] and Ex-Mt-B [Fig. S2(d)] reveal that Mt had been exfoliated into layers presenting POSS nanoparticles, with few layered structures.

As aforementioned, the pristine Mt and the In-Mt with layered structure presented the same $G(a)$ of Zhuralev–Lesokin–Tempelman equation, and the same $G(a)$ of Avrami–Erofeev equation for the Ex-Mt-A and the Ex-Mt-B with exfoliated structure. The E relates closely not only to the structures, but also to the weight loss. E is the required minimum energy of the molecules from a reactant state to an activated state in a chemical reaction. In the pyrolysis, it is the different energy between the onset point and the offset point. The pristine Mt and the In-Mt both had layered structures, with a basal space of 1.42 and 3.73 nm, respectively. The pyrolysis of pristine Mt was to remove the

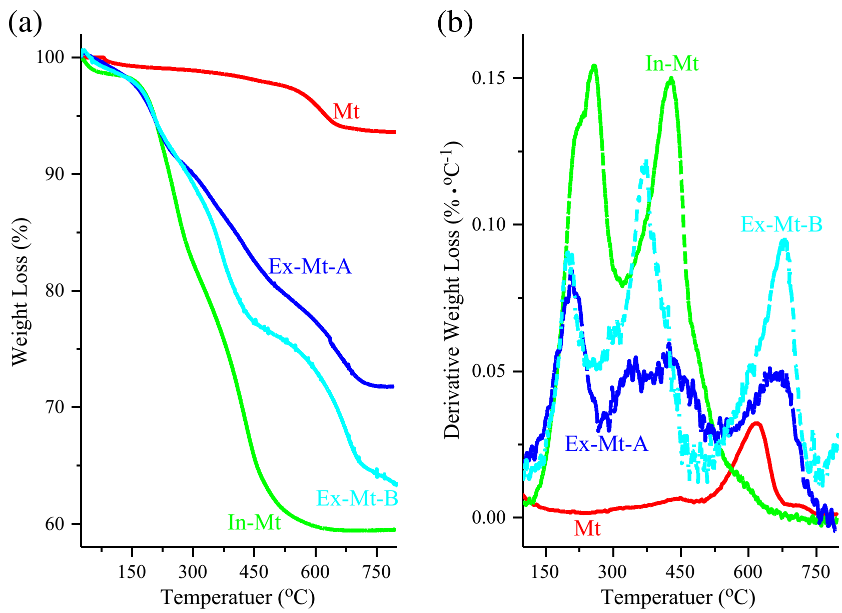

Fig. 2. (a) Weight loss and (b) derivative weight loss of Mt, In-Mt, Ex-Mt-A, and Ex-Mt-B.

crystal water between layers and the structural water in layers, generally needed much energy and could be performed at high temperatures, so the E was certainly high. While the pyrolysis of In-Mt was to remove the intercalator between layers, which was determined by the pyrolysis temperature of intercalator and could be accomplished more easily than to remove the crystal water between layers and the structural water in layers for pristine Mt. As Fig. 2(a) shows, the total weight loss of pristine Mt was 6% at temperatures up to 800 °C from the loss of physically absorbed water and crystal water between layers and the structural water in layers; the peak temperature (T_p) was 619 °C, and the derivative weight loss was 0.0322%·°C^{-1}, caused by the loss of crystal and structural water [Fig. 2(b)]. The weight loss of In-Mt at 40% was caused mainly by the pyrolysis of organic surfactant from *N*,*N*-dimethylstearylamine and propargyl bromide at temperatures up to 600 °C, at which point the intercalator had been pyrolyzed completely; the In-Mt displayed the T_p at 258 and 428 °C, corresponding to the derivative weight loss at 0.1543 and 0.1500%·°C^{-1} [Fig. 2(b)]. The derivative weight loss reflected the pyrolysis rate; the more the weight loss the higher the derivative weight loss. The T_p at 619 °C reveled the removing of the crystal water between layers and the structural water in layers for pristine Mt, and the T_p at 258 and 428 °C for removing the intercalator for In-Mt. Consequently, the former exhibited a high E at 613.59 kJ·mol^{-1}, and the latter at a low E of 87.04 kJ·mol^{-1} (Table 1).

For the Ex-Mt-A and Ex-Mt-B with exfoliated structure, their pyrolysis was not similar to that of pristine Mt and In-Mt. The monofunctionalized POSS presenting an organic substituent on the outer surface exfoliated Mt into single layers for Ex-Mt-A and the multifunctionalized POSS presenting eight organic substituents on the outer surfaces did that for Ex-Mt-B. The exfoliated structure and the different organic substituents on the outer surfaces of POSS molecules influenced the E, weight loss, and derivative weight loss significantly. The weight loss was about 28% for Ex-Mt-A and about 36% for Ex-Mt-B [Fig. 2(a)]. The Ex-Mt-A featured the T_p at 207, 424, and 663 °C with the corresponding derivative weight loss of 0.0846, 0.0595, and 0.0490%·°C^{-1}; the Ex-Mt-B at 199, 375, and 680 °C, with the corresponding derivative weight loss of 0.0903, 0.1201, and 0.0936%·°C^{-1} [Fig. 2(b)]. The T_p at 663 and 680 °C for Ex-Mt resulted from the collapse of POSS structures. For In-Mt, the intercalator was from *N*,*N*-dimethylstearylamine and propargyl bromide; for Ex-Mt, the organic substituent was also from them, and was connected to the outer surface of POSS nanoparticles through click chemistry (Cui and Kuo, 2012, 2013a,b, 2014). In other words, the pyrolysis of In-Mt was just to remove the intercalator, while that of Ex-Mt not only to remove the organic substituent but also to break the chemical bonds between organic substituent and POSS nanoparticles formed by click chemistry, so the In-Mt presented lower E than the Ex-Mt (Table 1). The Ex-Mt-A contained monofunctionalized POSS presenting an organic substituent on the outer surface, while the Ex-MT-B contained multi-functionalized POSS presenting eight organic substituents on the outer surfaces. During the pyrolysis, monochemical bond was broken for the Ex-Mt-A, while multichemical bonds were broken for the Ex-Mt-B; they all were formed by the click chemistry. In addition, more energy would be needed to accomplish the pyrolysis when the Ex-Mt contained higher organic content that was the weight loss. Therefore, the Ex-Mt-A showed a low E at 99.06 kJ·mol^{-1} and the Ex-Mt-B at a high E of 104.58 kJ·mol^{-1} (Table 1). The A, as shown in Table 1, displayed a similar variation trend to that of the E, which is a constant determined by the reaction and does not have any relationship to the reaction temperature and concentration in the system.

Table 1
Pyrolysis kinetics of Mt, In-Mt, Ex-Mt-A, and Ex-Mt-B.

	$G(a)$	E (kJ·mol^{-1})	A (min^{-1})	Reaction order
Mt	$\left[(1-a)^{-\frac{1}{3}}-1\right]^2$	613.59	2.88×10^{35}	2
In-Mt	$\left[(1-a)^{-\frac{1}{3}}-1\right]^2$	87.04	1.30×10^{6}	2
Ex-Mt-A	$[-\ln(1-a)]^4$	99.06	4.35×10^{6}	4
Ex-Mt-B	$[-\ln(1-a)]^4$	104.58	8.27×10^{6}	4

Table 2
Kinetic compensation effect equations of Mt, In-Mt, Ex-Mt-A, and Ex-Mt-B.

	Kinetic compensation effect equation	Correlation coefficient
Mt	$\ln A = 0.0001E - 1.5908$	0.9990
In-Mt	$\ln A = 0.0002E - 2.9985$	0.9786
Ex-Mt-A	$\ln A = 0.0002E - 3.5276$	0.8778
Ex-Mt-B	$\ln A = 0.0002E - 3.4927$	0.9039

In addition, the kinetic compensation effect is often used also in the kinetics. It indicates a linear relationship between ln$A$ and E that A compensates to the change of E partly (Hu and Shi, 2001):

$$\ln A = KE + Q$$

where K and Q are the kinetic compensation effect parameters calculated from the linear fit between E and A.

Table 2 shows the pyrolysis kinetic compensation effect equations of pristine Mt, In-Mt, Ex-Mt-A, and Ex-Mt-B. The pristine Mt is an inorganic mineral, while In-Mt, Ex-Mt-A, and Ex-Mt-B all contained organics. Therefore, the K was the same at 0.0002 for In-Mt, Ex-Mt-A, and Ex-Mt-B, which was different from that of pristine Mt at 0.0001. The Q had a close relationship to the layered structures for pristine Mt and In-Mt, and the exfoliated structures and cage-like molecules of POSS nanoparticles for Ex-Mt-A and Ex-Mt-B. It varied similarly to that of E and A. Because the K and Q are not affected by experimental factors, the kinetic compensation effect equations can explain the pyrolysis processes and reveal the pyrolysis of pristine Mt, In-Mt, Ex-Mt-A, and Ex-Mt-B clearly, and also are their theoretical expressions.

4. Conclusions

In this study, the pyrolysis kinetics of Ex-Mt from pristine Mt, functionalized POSS, and click chemistry was investigated, which had a close relationship to the layered structures, exfoliated structures, and cage-like molecules of POSS nanoparticles. The pristine Mt and In-Mt had the same $G(a)$ of Zhuralev–Lesokin–Tempelman equation, and the $G(a)$ for Ex-Mt-A and Ex-Mt-B both was Avrami–Erofeev equation. The kinetic compensation effect equations revealed the pyrolysis of pristine Mt, In-Mt, Ex-Mt-A and Ex-Mt-B.

Appendix A. Supplementary data

Supplementary data to this article can be found online at http://dx.doi.org/10.1016/j.clay.2014.09.026.

References

Agrawal, R.K., 1987. A new equation for modeling nonisothermal kinetics. J. Therm. Anal. 32, 149–156.

Bee, S.T., Hassan, A., Ratnam, C.T., Tee, T.T., Sin, L.T., 2012. Effects of montmorillonite on the electron beam irradiated alumina trihydrate added polyethylene and ethylene vinyl acetate nanocomposite. Polym. Compos. 33, 1883–1892.

Chen, X.L., Jiao, C.M., Zhang, J., 2012. Thermal and combustion behavior of ethylene-vinyl acetate/aluminum trihydroxide/Fe-montmorillonite composites. Polym. Eng. Sci. 52, 414–419.

Cui, H.W., Du, G.B., 2011a. Preparation and characterization of PVAc–MMT–DOAB. High Perform. Polym. 23, 40–48.

Cui, H.W., Du, G.B., 2011b. Rheology of PVAc–MMT–STAB. J. Adhes. Sci. Technol. 25, 1671–1679.

Cui, H.W., Du, G.B., 2011c. Development of an exfoliated nanocomposite prepared by vinyl acetate and organic montmorillonite: structure, dynamic mechanical properties and thermal degradation. Compos. Interf. 18, 557–573.

Cui, H.W., Du, G.B., 2012a. Preparation and characterization of exfoliated nano-composite prepared by vinyl acetate, montmorillonite and dioctadecyl dimethyl ammonium bromide. E-Polym. 002, 1–11.

Cui, H.W., Du, G.B., 2012b. Preparation and characterization of exfoliated nanocomposite of polyvinyl acetate and organic montmorillonite. Adv. Polym. Technol. 31, 130–140.

Cui, H.W., Du, G.B., 2012c. Development of exfoliated nanocomposite prepared from vinyl acetate and montmorillonite. Plast. Rubber Compos. 41, 413–417.

Cui, H.W., Du, G.B., 2012d. Using Agrawal integral equation to study the glass transition and cold crystallization kinetics of exfoliated nano-composites synthesized by vinyl acetate and organic montmorillonite. J. Compos. Mater. 46, 2951–2958.

Cui, H.W., Du, G.B., 2013a. Influence of different synthesis processes on the rheology of PVAc–MMT–DOAB exfoliated nano-composite. Iran. Polym. J. 22, 165–173.

Cui, H.W., Du, G.B., 2013b. Structure and dynamic mechanical kinetics of polyvinyl acetate–montmorillonite–dioctadecyl dimethyl ammonium bromide. J. Thermoplast. Compos. Mater. 26, 1206–1222.

Cui, H.W., Du, G.B., 2013c. Pyrolysis properties of exfoliated nanocomposite synthesized by vinyl acetate and organic montmorillonite through different processes. J. Thermoplast. Compos. Mater. 26, 156–175.

Cui, H.W., Kuo, S.W., 2012. Using a polyhedral oligomeric silsesquioxane surfactant and click chemistry to exfoliate montmorillonite. RSC Adv. 2, 12148–12152.

Cui, H.W., Kuo, S.W., 2013a. Using Agrawal integral equation and thermogravimetric analysis (TGA) to study the pyrolysis kinetics of nanocomposites of polybenzoxazine and exfoliated montmorillonite from a mono-functionalized azide polyhedral oligomeric silsesquioxane and click chemistry. Polym. Bull. 70, 3143–3153.

Cui, H.W., Kuo, S.W., 2013b. Nanocomposites of polybenzoxazine and exfoliated montmorillonite using a polyhedral oligomeric silsesquioxane surfactant and click chemistry. J. Polym. Res. 20 (114 (13 pages)).

Cui, H.W., Kuo, S.W., 2014. Using Agrawal integral equation, dynamic mechanical analysis (DMA), and differential scanning calorimeter (DSC) methods to study the glass transition kinetics of nanocomposites of polybenzoxazine and exfoliated montmorillonite from a polyhedral oligomeric silsesquioxane surfactant and click chemistry. Appl. Clay Sci. 91–92, 1–5.

Demir, K.D., Tasdelen, M.A., Uyar, T., Kawaguchi, A.W., Sudo, A., Endo, T., Yagci, Y., 2011. Synthesis of polybenzoxazine/clay nanocomposites by in situ thermal ring-opening polymerization using intercalated monomer. J. Polym. Sci. A 49, 4213–4220.

Dolomanova, V., Kumar, V., Pyrz, R., Madaleno, L.A.O., Jensen, L.R., Rauhe, J.C.M., 2012. Fabrication of microcellular PP–MMT nanocomposite foams in a sub-critical CO_2 process. Cell. Polym. 31, 125–143.

Fang, Q., Cui, H.W., Du, G.B., 2013. Using the Agrawal integral equation to study the thermal degradation of polyvinyl acetate–montmorillonite–dioctadecyl dimethyl ammonium bromide. J. Polym. Eng. 33, 41–47.

Fu, H.K., Huang, C.F., Kuo, S.W., Lin, H.C., Yei, D.R., Chang, F.C., 2008. Effect of an organically modified nanoclay on low-surface-energy materials of polybenzoxazine. Macromol. Rapid Commun. 29, 1216–1220.

Greesh, N., Sanderson, R., Hartmann, P.C., 2012. Preparation of polystyrene colloid particles armored by clay platelets via dispersion polymerization. Polymer 53, 708–718.

Ha, S.R., Rhee, K.Y., Shin, H., 2008. Effect of MMT concentration on tribological behavior of MMT/epoxy nanocomposite. J. Nanosci. Nanotechnol. 8, 4869–4872.

Hu, R.Z., Shi, Q.Z., 2001. Thermal Analysis Kinetics. Science Press, Beijing, pp. 52–53.

Hwang, S.S., Liu, S.P., Hsu, P.P., Yeh, J.M., Yang, J.P., Chen, C.L., 2012. Morphology, mechanical, and rheological behavior of microcellular injection molded EVA–clay nanocomposites. Int. Commun. Heat. Mass. 39, 383–389.

Lakshmi, A.S., Narmadha, B., Redd, B.S.R., 2008. Enhanced thermal stability and structural characteristics of different MMT–clay/epoxy-nanocomposite materials. Polym. Degrad. Stab. 93, 201–213.

Liang, G.D., Xu, J.T., Xu, W.B., 2004. PE/PE-g-MAH/Org-MMT nanocomposites. II. Nonisothermal crystallization kinetics. J. Appl. Polym. Sci. 91, 3054–3059.

Liu, Y., Wang, J.S., Deng, C.L., Wang, D.Y., Song, Y.P., Wang, Y.Z., 2010. The synergistic flame-retardant effect of O-MMT on the intumescent flame-retardant PP/CA/APP systems. Polym. Adv. Technol. 21, 789–796.

Martin, Z., Jimenez, I., Gomez, M.A., Ade, H., Kilcoyne, D.A., 2010. Interfacial interactions in PP/MMT/SEBS nanocomposites. Macromolecules 43, 448–453.

Nuhiji, B., Attard, D., Thorogood, G., Hanley, T., Magniez, K., Fox, B., 2011. The effect of alternate heating rates during cure on the structure–property relationships of epoxy/MMT clay nanocomposites. Compos. Sci. Technol. 71, 1761–1768.

Qian, J.H., Guo, C.Y., Wang, H., Hu, Y.L., 2007. Fabrication and characterization of PE/MMT nanocomposites via copolymerization of ethylene and in situ formed alpha-olefins. J. Mater. Sci. 42, 4350–4355.

Qiao, M., Ran, Q.P., Wu, S.S., Shen, J., 2009. A study of PU/MMT nanocomposites. Polym. Polym. Compos. 17, 91–96.

Takeichi, T., Zeidam, R., Agag, T., 2002. Polybenzoxazine/clay hybrid nanocomposites: influence of preparation method on the curing behavior and properties of polybenzoxazines. Polymer 43, 45–53.

Teixeira, R.F.A., McKenzie, H.S., Boyd, A.A., Bon, S.A.F., 2011. Pickering emulsion polymerization using laponite clay as stabilizer to prepare armored “soft” polymer latexes. Macromolecules 44, 7415–7422.

Touchaleaume, F., Soulestin, J., Sclavons, M., Devaux, J., Lacrampe, M.F., Krawczak, P., 2011. One-step water-assisted melt-compounding of polyamide 6/pristine clay nanocomposites: an efficient way to prevent matrix degradation. Polym. Degrad. Stab. 96, 1890–1900.

Vengatesan, M.R., Devaraju, S., Dinakaran, K., Alagar, M., 2011. Studies on thermal and dielectric properties of organo clay and octakis (dimethylsiloxypropylglycidylether) silsesquioxane filled polybenzoxazine hybrid nanocomposites. Polym. Compos. 32, 1701–1711.

Wang, C.H., Shieh, Y.T., Nutt, S., 2009. The effects of soft-segment molecular weight and organic modifier on properties of organic-modified MMT–PU nanocomposites. J. Appl. Polym. Sci. 114, 1025–1032.

Xu, W.B., Zhai, H.B., Guo, H.Y., Zhou, Z.F., Whitely, N., Pan, W.P., 2004. PE/ORG-MMT nanocomposites—non-isothermal crystallization kinetics. J. Therm. Anal. Calorim. 78, 101–112.

Yu, H., Ran, Q., Wu, S., Shen, J., 2008. Structure and property of PU/MMT nanocomposites by in-situ polymerization. Polym. Plast. Technol. Eng. 47, 619–622.

Zhang, C., Tjiu, W.W., Fan, W., Yang, Z., Huang, S., Liu, T.X., 2011. Aqueous stabilization of graphene sheets using exfoliated montmorillonite nanoplatelets for multifunctional free-standing hybrid films via vacuum-assisted self-assembly. J. Mater. Chem. 21, 18011–18017.

Zhu, W.J., Lu, C.H., Chang, F.C., Kuo, S.W., 2012. Supramolecular ionic strength-modulating microstructures and properties of nacre-like biomimetic nanocomposites containing high loading clay. RSC Adv. 2, 6295–6305.